First-principles calculations of the phonon, mechanical and Thermoelectric properties of half-Heusler alloy VIrSi alloys

Paul O. Adebambo[1,a], Bamidele I. Adetunji[2], Oghenekevwe T. Uto[3], Stephane Kenmoe[4,a] and Gboyega A. Adebayo[1,a]

[1] *Department of Physics, Federal University of Agriculture, PMB 2240 Abeokuta, Nigeria*

[2] *Department of Physics, Bells University of Technology, Ota, Nigeria*

[3] *Department of Physics, The University of the Gambia, Kanifing, Gambia and*

[4] *Department of Theoretical Chemistry, University of Duisburg-Essen, Universitätsstr. 2, D-45141 Essen, Germany*

(Dated: November 22, 2022)

The density functional theory was used to explore the structural, electronic, dynamical, and thermoelectric properties of a VIrSi Half-Heulser (HH) alloy. The minimum lattice constant of 5.69 (Å) was obtained for VIrSi alloy. Besides, the band structure and the projected density of states for this HH alloy were calculated, and the gap between the valence and conduction bands was noted to be 0.2 eV. Also, the quasi-harmonic approximation was used to predict the dynamical stability of the VIrSi HH alloy. At 300 K, the Seebeck Coefficient of 370 and -270 $\mu V.K^{-1}$., respectively, was achieved for the p and n-type doping. From the power factor result, the highest peak of 18 X $10^{11} W/cm.K^2$ is obtained in the n-type doping. The Figure of Merit (ZT) result revealed that VIrSi alloy possesses a high ZT at room temperature, which would make VIrSi alloy applicable for thermoelectric performance.

Keywords: Phonon dispersion, PDOS, Mechanical properties, Power factor and Figure of Merit

[a] authors to whom all correspondences can also be sent: adebambo@physics.unaab.edu.ng; stephane.kenmoe@uni-due.de; adebayo@physics.unaab.edu.ng

 doi:10.20944/preprints202211.0409.v1

I. INTRODUCTION

Since the last century, the global demand for energy has considerably expanded. Climate change, which adversely affects the depletion of fossil resources and leads to an energy crisis, is one of the causes of this need. However, to meet this problem, experts are attempting to increase the efficiency of environmentally friendly technology such as biomass, solar photovoltaic, wind turbines, and thermoelectric. Due to its ability to convert heat into electricity and vice versa, thermoelectric (TE) materials have attracted extensive research in an effort to meet this technology's demands. A dimensionless figure of merit, $Z_T = (S^2\sigma T)/K$, is typically used to assess a material TE performance. Where S, σ, K and T stand for the Seebeck coefficient, electrical conductivity, total thermal conductivity (which includes lattice and electronic thermal conductivity), and absolute operating temperature, respectively. Due to their relatively high Seebeck coefficient, Heusler alloys are among the most promising thermoelectric materials[1–5].

The wide family of Heusler alloys, which Fritz Heusler initially described in 1903, has qualities that can be altered to suit technological applications in numerous fields of science and engineering research. The half-Heusler (HH) is one of a separate category that they are divided into[6]. These half-Heusler alloys typically have some distinctive qualities that set them apart from other kinds of Heusler alloys. They typically have 18 valence electrons with a small band gap, which is one of these characteristics. By substituting at different crystal locations, it is possible to change the thermoelectric efficiency of half-Heusler compounds and achieve the ideal balance of Seebeck, electric resistivity, and thermal conductivity ([7–14]. In turn, this might lower these alloys lattice thermal conductivity and raise their power factor. Thereby making them become ideal for thermoelectric applications.

Numerous researchers have looked into the thermoelectric properties of various Half-Heusler compounds in the past and in the present using both experimental and theoretical techniques. For instance, due to their Figure of Merit of 0.7 citeShen,Cui the Half-Heusler alloys MNiSn (M = Ti, Zr, and Hf) have been touted as one of the promising materials for thermoelectric technology. Here, they replace Ni with Pd in a methodical way such that solid-state reactions can be used to create the samples. High-quality component powder is heated for 96–168 hours in a flowing argon atmosphere to 1173 K. FeXSb (X = V, Nb) has also been reported to have a high power factor and Seebeck coefficient at room temperature[16–20]. For these materials, X-ray diffraction (XRD) was used on a RigakuD/MAX-2550PC diffractometer to identify the samples' phase structures. The samples have no impurity phases, according to the XRD examination.

In order to calculate the structural, electrical, elastic, and thermoelectric properties of novel HfPtPb HH alloys, Kaur and Rai recently used density functional theory with semi-classical Boltzmann transport equations under the constant relaxation time approach. This alloy is mechanically and dynamically stable, according to their report. Additionally, it was discovered that for this material, the n-type doing produced the maximum Seebeck coefficient. Within an enhanced TB-mBJ potential, Wang and Wang used first-principles simulations to examine the electronic structure and thermoelectric characteristics of half-Heusler semiconductors ABPb (A = Hf, Zr; B = Ni, Pd) l[22]. Using Boltzmann transport theory, they calculated Seebeck and power factor within the constant relaxation time as well as projected the band structure for both p- and n-type doped compounds. According to their findings, all of the compounds are semiconductors with a narrow bandgap. Additionally, they stated that their power factors closely match the outcomes of the experiment and offered some suggestions for improving the thermoelectric properties.

The ternary intermetallic Full- and Half-Heusler alloys have stoichiometric compositions of X2YZ and XYZ, re-

 doi:10.20944/preprints202211.0409.v1

spectively. These classifications are done such that the X and Y elements are transitions metals, while the Z elements are semiconductor or sp atoms. Nevertheless, our choice of VIrSi alloy conforms with this arrangement. However, we have carefully noted that only a little work had been conducted on this alloy. Furthermore, the high thermoelectric properties that usually characterize the undoped HH alloys is one of the motivation to explore additional research on HH compounds. To our knowledge, one of such compound is VIrSi alloy, for which extensive investigations, including calculation of structural, electronic, elastic, dynamical, and thermoelectric properties are scare. Consequently, we have made used the density functional theory as well as semi-classical Boltzmann transport theory within the constant rigid band approximation to investigate the structural, mechanical, electrical, and thermoelectric properties of VIrSi alloy.

II. COMPUTATIONAL PROCEDURE

The pseudopotential plane wave method within density functional theory, as implemented in the Quantum Espresso simulation code[24-26], was used to calculate the structural and electrical properties of this alloy. The exchange correlation functional was approximated using the Generalized Gradient Approximation (GGA)[27] with Perdew Burke-Ernzerhof (PBE). The kinetic energy cut-off of 40 Ry was adopted for this calculations, while a 6 x 6 x 6 grid in the Monkhorst-Pack[28] scheme was constructed for the electronic structure calculation. In order to confirm the convergence of the results, we set a 10^{-4} Ry criterion for convergence of the total energy. The plane wave pseudopotential (PWPP) basis sets consists of the $3d^2$ $4s^2$, $3s^2$ $3p^2$, $5d^7$ $6s^2$ states for V, Si, and Ir, respectively. The plane wave pseudopotential (PWPP) basis sets which consists of the $3d^2$ $4s^2$, $3s^2$ $3p^2$, $5d^7$ $6s^2$ states for V, Si, and Ir, respectively were used for all these calculations. While, a denser k-point mesh of (12 x 12 x 12) grid was used to calculate the electronic density of states (DOS) with a tetrahedra occupation switched on. By fitting the results of the total energy computation to the Birch-Murnaghan equation of states, we were able to extract the majority of the pertinent information concerning the structural behavior of the alloys[29-30].

III. RESULTS AND DISCUSSION

A. Structural and Electronic Properties

We carried out a number of self-consistent computations in order to optimize the crystal structure of VIrSi half-Heusler alloys. This alloy is known to crystallize in $C1_b$ structure with space group $F43m$, where Si atoms are placed at 0.00 0.00 0.00 position. The Ir atom is located at 0.25 0.25 0.25, and the V atom occupies the atomic position 0.50 0.50 0.50 in the crystal, as shown in Figure 1a. From here, we can see that each V atom is placed in between the Si atoms at the edges. At the same time, Ir atoms are bonded by both the Si and V atoms. In Figure 1b, the total energy of VIrSi alloys as a function of lattice parameters within the GGA approximations is shown. These lattice parameters were also fitted in Murnaghan's equation of state (EOS), and the results were also plotted along with the calculated lattice parameters in Fig. 1b. Besides, we used the fitted in Murnaghan's equation of state (EOS) minimum lattice constant a, bulk modulus B_0 and its pressure derivatives $B_0^{'}$ for this alloy and these results are tabulated in Table I.

Preprints (www.preprints.org) | NOT PEER-REVIEWED | Posted: 22 November 2022 doi:10.20944/preprints202211.0409.v1

The band structure and projected density of state (PDOS) of VIrSi alloys are presented in Figure 2. The dotted line in Figure 2a at 0 eV is the Fermi energy level which separates the valence band from the conduction band. This band structure is depicted along the high symmetry points $\Gamma \rightarrow X \rightarrow W \rightarrow K \rightarrow \Gamma \rightarrow L \rightarrow U \rightarrow W \rightarrow L \rightarrow U$. From here, we notice that the upper valence band is located at W, while the lower conduction band is at X. Consequently, VIrSi alloys have a narrow indirect bandgap of 0.2 eV. The origin of this bandgap in the half Heusler 18 valence electrons has previously been provided in detail by Galanakis et al.[33] Besides, this energy bandgap corroborates with the results of the PDOS presented in Fig. 2b. it is seen from this PDOS calculations that Iridium s and d-orbitals contributed to both the conduction and valence bands. The contribution of silicon s-orbital and the contribution of the Vanadium p-orbital is not well pronounced in both conduction and valence bands.

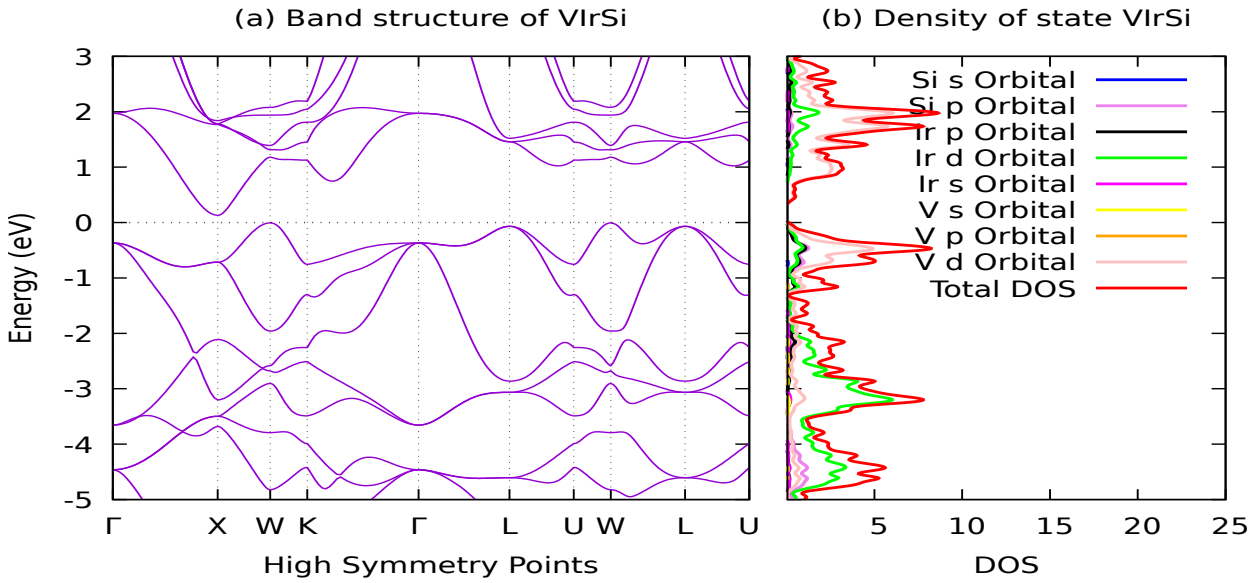

FIG. 2. Electronic band structure and Projected Density of state of VIrSi

TABLE I. Optimization of Lattice parameter a, bulk modulus B, and pressure derivative of bulk modulus B' of VIrSi.

Materials	Methods	a(Å)	$B(GPa)$	B'
VIrSi	Present Work	5.69	218.3	4.22
	Experiment		-	-

B. Phonon dispersion curve of VIrSi Half-Heusler alloys

The Phonon dispersion curves along the Brillouin zone $K \rightarrow \Gamma \rightarrow L \rightarrow U \rightarrow \Gamma \rightarrow W \rightarrow X \rightarrow \Gamma$ path were generated using Phonopy code[34,44] within the the quasi-harmonic approximation[45] and are displayed in Figure 3. The dispersion in Figure 3 can be classified into the upper (optical) and lower (acoustic) modes. The acoustic modes lie in between 0 and 5.70 THz, while the optical mode extend from 6.93 to 11.38 THz. Both the optical and acoustic branches are separated. The former shows three acoustic modes, while the later, which contains both the longitudinal optical (LO)

Preprints (www.preprints.org) | NOT PEER-REVIEWED | Posted: 22 November 2022 doi:10.20944/preprints202211.0409.v1

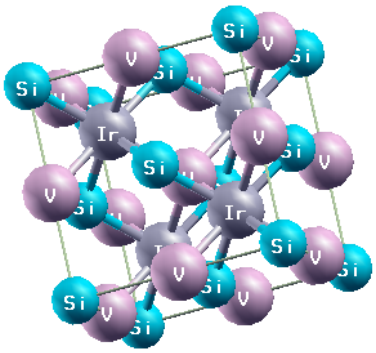

(a)

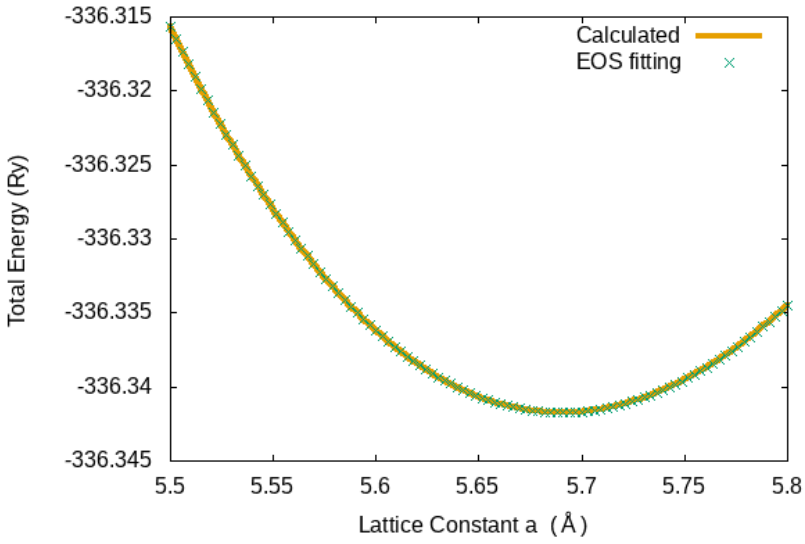

(b)

FIG. 1. (a) The crystal structure and (b) optimization of the lattice parameters of VIrSi Half-Heusler alloy.

and transverse optical (TO) modes, shows three branches for each of them. Our calculated phonon frequencies values for LO (Γ) is 9.43 THz and 7.68 THz for TO (Γ). In the acoustic branch, the calculated longitudinal acoustic is found to be 5.65 THz while the transverse acoustic is obtained to be 3.90 THz. In the optical mode, which is predominantly dominated by the states V (Z = 23) and Si (Z = 14), we observed splitting at the Γ point. At the same time, the state of the heavier atom Ir (Z = 77) is placed in the acoustic modes of the spectrum. The absence of negative frequency

Preprints (www.preprints.org) | NOT PEER-REVIEWED | Posted: 22 November 2022 doi:10.20944/preprints202211.0409.v1

in Fig. 3 implies that VIrSi alloy is dynamically stable.

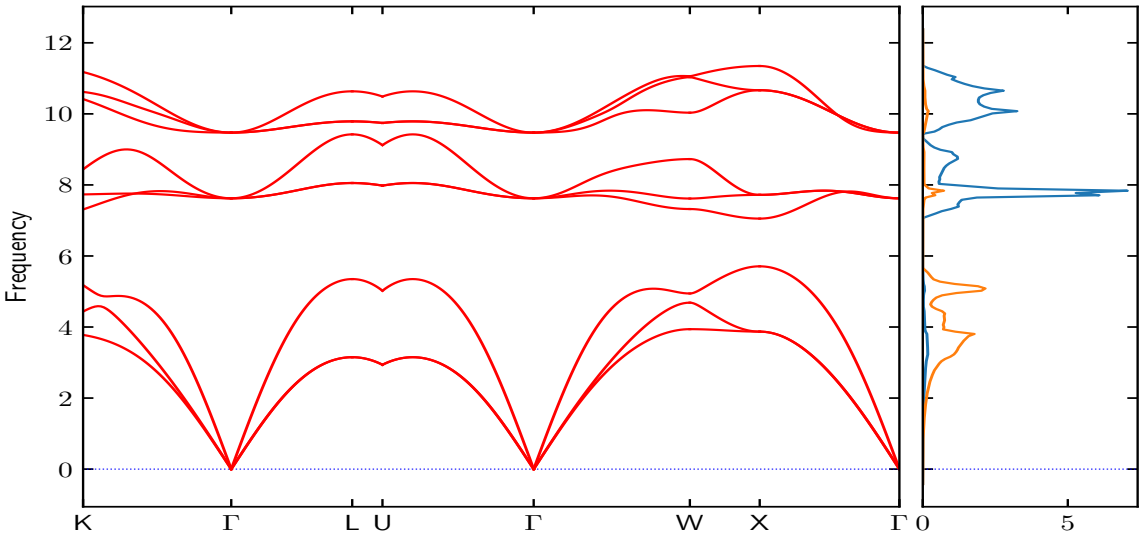

FIG. 3. (a) Calculated phonon dispersion curve and (b) VDOS of VIrSi alloy

C. Thermoelectric Properties of VIrSi Half-Heusler alloys

In Figure 4, the power factor, electrical conductivity and the Seebeck coefficient with respect to energy at different temperature ranges are presented. In Figure 4a, the power factor variation with energy at different temperatures is clearly depicted. This power factor shows the performance of VIrSi as a thermoelectric material. The maximum value of the power factor is obtained at 18 X $10^{11} W/cm.K^2$.s for the n-type doping, at 800 K. While, for the p-type doping 6 X $10^{11} W/cm.K^2$.s is noted to be the maximum power factor also at 800 K. Meanwhile, at 300 K, the maximum power factor of 4 X $10^{11} W/cm.K^2$.s and 2 X $10^{11} W/cm.K^2$.s were noted for n-type and p-type respectively.

Preprints (www.preprints.org) | NOT PEER-REVIEWED | Posted: 22 November 2022 doi:10.20944/preprints202211.0409.v1

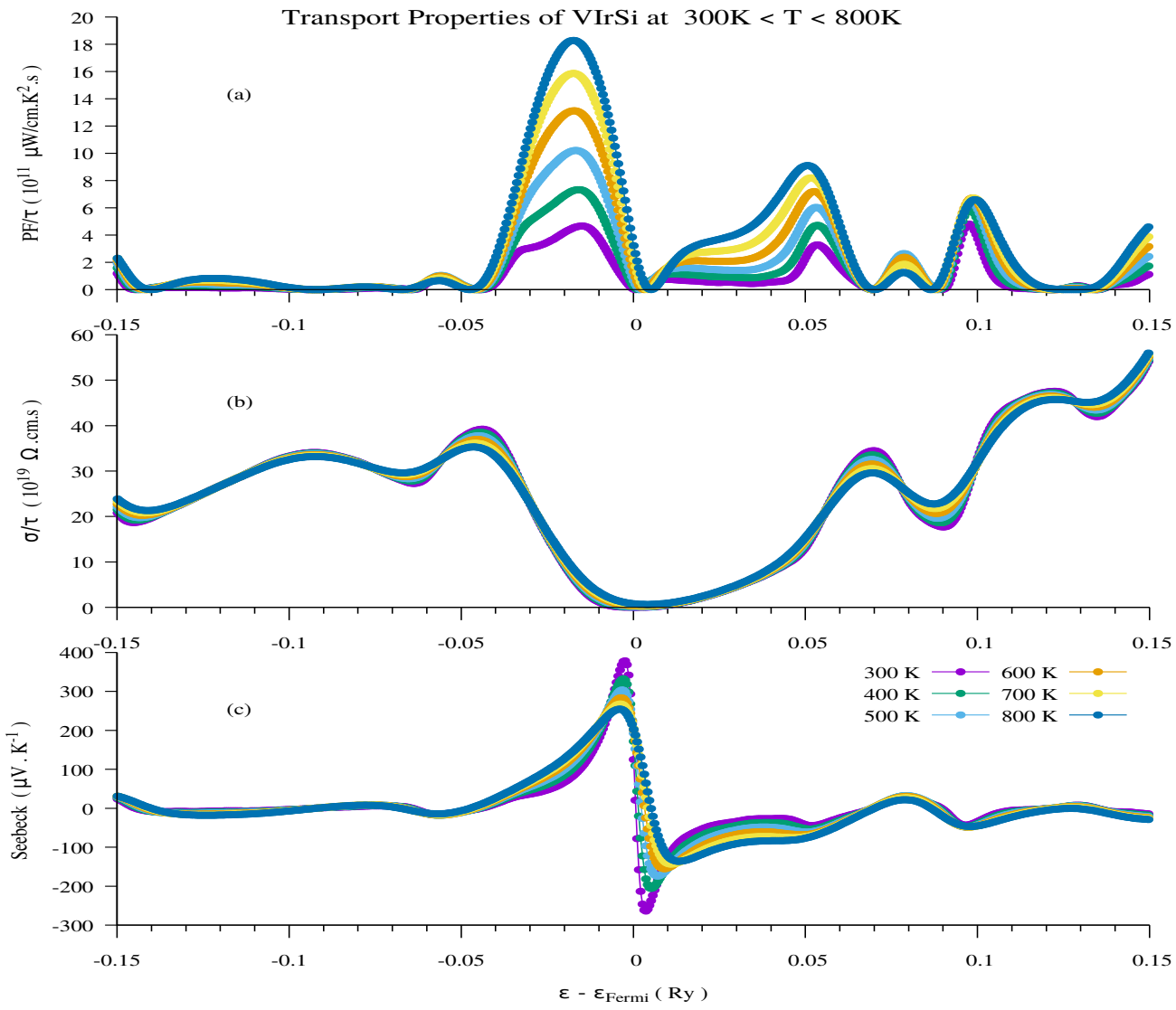

FIG. 4. (a) Power factor, (b) Electrical conductivity, and (c) Seebeck Coefficient of VIrSi Half-Heusler alloys

Preprints (www.preprints.org) | NOT PEER-REVIEWED | Posted: 22 November 2022 doi:10.20944/preprints202211.0409.v1

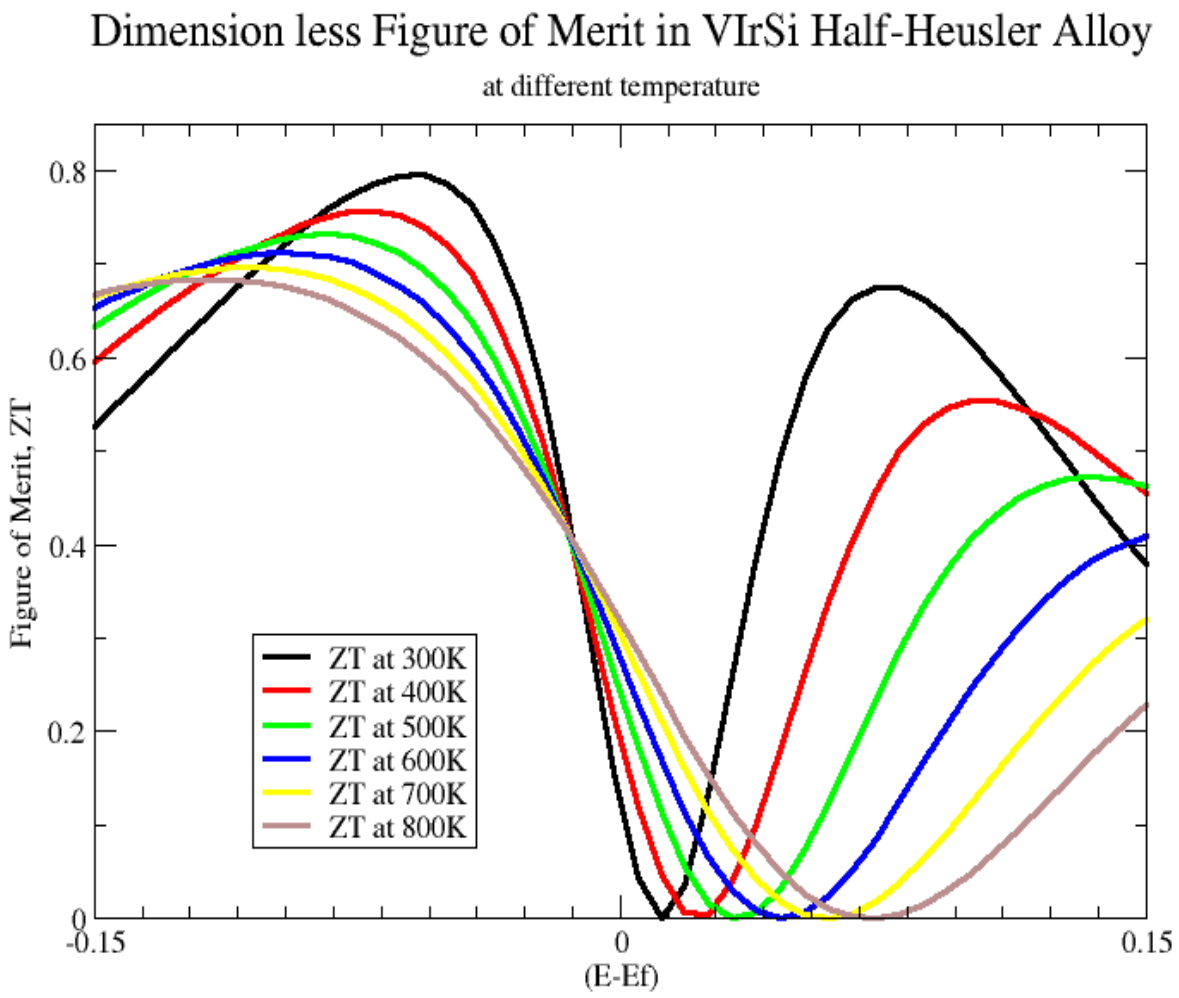

FIG. 5. High Figure of Merit in VIrSi Half-Heusler alloys from 300 to 800K

Figure 4b presented the variation in electrical conductivity per relaxation time as a function of energy and temperature. At all temperatures, the electrical conductivity per relaxation time exhibits a consistent pattern. Electrical conductivity per relaxation time has a greater gradient for positively increasing energies than for more negative energies. Thus, n-type compositions have a lower electrical conductivity than p-type compositions. Electrical conductivity per relaxation time is zero in the energy range -0.005 to +0.005. However, the value grows beyond this range.

As shown in Figure 4c, the Seebeck coefficient at the doping of p-type and n-type materials first increased as the energy increased before reaching a maximum value and decreased drastically as it can be seen from the peaks in the energy range of -0.005 and +0.005. The curves intend to be at zero outside this range. The peak maximum for the p-type doping of VIrSi alloy is found at 370 $\mu V.K^{-1}$. while the peak maximum for the n-type doping is observed at -270 $\mu V.K^{-1}$. The peaks are observed at room temperature, indicating that VIrSi alloy has an excellent thermoelectric trait. The peaks heights tend to be reduced as the temperature rises. The present calculated values of the Seebeck

 doi:10.20944/preprints202211.0409.v1

coefficient of VIrSi alloys at 300 K was compared with other half-Heusler alloys VruSb (+262.67 $\mu V.K^{-1}$), NbRuSb (199.88 $\mu V.K^{-1}$) and TaRuSb (181.5 $\mu V.K^{-1}$)[21]. We conclude that VirSi has the highest value of the Seebeck coefficient in this regard.

In Figure 5, the dimension less Figure of Merit is plotted against the chemical potential at each temperature. It is puzzling that, even at room temperature, VIrSi possesses a high Figure of Merit, ZT ≈ 0.8 in the n-type and ≈ 0.68 in the p-type compound. We observe a decrease in the value of ZT as temperature increases and we attribute this to the strong effects of phonon contribution to the thermal conductivity κ.

IV. CONCLUSION

We used the density functional theory and semi-classical Boltzmann transport theory under the constant rigid band approximation to predict the structural, electrical, dynamical, and thermoelectric properties of VIrSi alloy in order to have more insight into these properties. For this alloy, we calculated a lattice constant of 5.69 (Å). The band structure and the projected density of the State of VIrSi alloys were also reported in this work. The contributions of Iridium s and d-orbitals is significant both the conduction and valence bands. Also, we found that the optical and acoustic branches are separated in the Phonon dispersion curve. While the absence of negative frequency in the phonon dispersion curve implies that VIrSi alloy is dynamical stable. To measure the thermoelectric performance of VIrSi alloy, we calculated the Seebeck coefficient, electrical conductivity, the power factor and the dimensionless Figure of Merit. At room temperature, the peak maximum obtained from the calculated Seebeck coefficient is 370 $\mu V.K^{-1}$ for the p-type doping while -270 $\mu V.K^{-1}$ is deduced from the n-type doping. Additionally, our findings indicate that n-type compositions have a lower electrical conductivity than p-type compositions. Besides, the power factor of 4 X $10^{11} W/cm.K^2$.s was obtained for the n-type doping while PF of 2 X $10^{11} W/cm.K^2$.s was also achieved p-type doping at room temperature, which implies that VIrSi alloy can be applicable for thermoelectricity. In addition, the high values of both the n- and p-type VIrSi is in an indication of its applicability as a power generator.

ACKNOWLEDGEMENT

SK gratefully acknowledges the Deutsche Forschungsgemeinschaft (DFG, German Research Foundation)—388390466—TRR 247 (2018). Three of us, POA, BIA and GAA, acknowledge support of CINECA for computational facilities under the Project HPC-EUROPA3 (INFRAIA-2016-1-730897), with the support of the EC Research Innovation Action under the H2020 Programme.

[1] D.M.Rowe, CRC Handbook of Thermoelectrics, CRC Handbook of Thermoelectrics. CRC Press, 1995, *doi* : 10.1201/9781420049718.

[2] M. G. Kanatzidis, Nanostructured thermoelectrics: The new paradigm, Chemistry of Materials, vol. 22, no. 3. pp. 648–659, Feb. 09, 2010, doi:10.1021/cm902195j.

[3] X.F. Zheng, C.X. Liu, Y.Y. Yan, Q. Wang, Renew. Sustain. Energy Rev. 32 (2014) 486.

[4] G.S. Nolas, J. Poon, M. Kanatzidis, MRS Bull. 31 (2006) 199.

[5] L. D. Zhao, V. P. Dravid, and M. G. Kanatzidis, "The panoscopic approach to high performance thermoelectrics," Energy and Environmental Science, vol. 7, no. 1. Royal Society of Chemistry, pp. 251–268, 2014, *doi* : 10.1039/*c*3*ee*43099*e*.

[6] O. T. Uto, P.O. Adebambo, J.O.Akinlami, S. Kenmoe, and G.A.Adebayo, Solids, (2022) 3(1), pp.22-33.

[7] N. Shutoh, S. Sakurada, J. Alloys Compd. 389 (2005) 204.

[8] S.R. Culp, S.J. Poon, N. Hickman, T.M. Tritt, J. Blumm, Appl. Phys. Lett. 88 (2006) 042106.

[9] S.-W. Kim, Y. Kimura, Y. Mishima, Intermetallics 15 (2007) 349.

[10] S. Katsuyama, R. Matsuo, M. Ito, J. Alloys Compd. 428 (2007) 262.

[11] Sakurada, S. and Shutoh, N. Effect of Ti substitution on the thermoelectric properties of (Zr,Hf)NiSn half-Heusler compounds. Appl. Phys. Lett. 86, 3159 (2005).

[12] Yu, C. et al, High-performance half-Heusler thermoelectric materials Hf1-xZrxNiSn1-ySby prepared by levitation melting and spark plasma sintering. Acta Mater 57, 2757–2764 (2009).

[13] Shen, Q. et al. Effects of partial substitution of Ni by Pd on the thermoelectric properties of ZrNiSn-based half-Heusler compounds. Appl. Phys. Lett. 79, 4165–4167 (2001).

[14] Zhang, H. et al, Thermoelectric properties of n-type half-Heusler compounds $(Hf_{0.25}Zr_{0.75})1 - xNb_xNiSn$. Acta Mater. 113, 41–47(2016).

[15] Cui Yu, Tie-Jun Zhu, Rui-Zhi Shi, et al., Acta Mater. 57 (2009) 2757.

[16] C.G. Fu, H.H. Xie, Y.T. Liu, et al., Intermetallics 32 (2013) 39.

[17] C.G. Fu, H.H. Xie, T.J. Zhu, J. Xie, X.B. Zhao, J. Appl. Phys. 112 (2012) 124915.

[18] C.G. Fu, T.J. Zhu, Y.Z. Pei, et al., Adv. Energy Mater. (2014) 1400600.

[19] C.G. Fu, T.J. Zhu, Y.T. Liu, et al., Energy Environ. Sci. 8 (2015) 216C220.

[20] C.G. Fu, Y.T. Liu, H.H. Xie, et al., J. Appl. Phys. 114 (2013) 134905.

[21] K. Kaur, and D. P. Rai, R. K. Thapa and S. Srivastava: J. Appl Phys. 122 045110 (2017).

[22] G. Wang and D. Wang, J. Alloys Compd., 682, 375-380 (2016).

[23] R. W. G. Wyckoff, Crystal Structures, 2nd ed., Vol. 1 (John Wiley & Sons, 1963).

[24] S. Scandolo, P. Giannozzi, C. Cavaoni, S. de Gironcoli, A. Pasquarello and S. Baroni, Z. Kristallogr, 220 (2005) 574579.

[25] P. Giannozzi, S. Baroni, N. Bonini, M. Calandra, R. Car, C. Cavazzoni, D. Ceresoli, G. L. Chiarotti, M. Cococcioni, I. Dabo, A. D. Corso, S. de Gironcoli, S. Fabris, G. Fratesi, R. Gebauer, U. Gerstmann, C. Gougoussis, A. Kokalj, M. Lazzeri, L. Martin-Samos, N. Marzari, F. Mauri, R. Mazzarello, S. Paolini, A. Pasquarello, L. Paulatto, C. Sbraccia, S. Scandolo, G. Sclauzero, A. P. Seitsonen, A. Smogunov, P. Umari, R. M. Wentzcovitch, J. Phys.:Condens. Matter 21 (39) (2009) 395502.

[26] P. Giannozzi, O. Andreussi, T. Brumme, O. Bunau, M. Buongiorno Nardelli, M. Calandra, R. Car, C. Cavazzoni, D. Ceresoli, M. Cococcioni, N. Colonna, I. Carnimeo, A. Dal Corso, S. de Gironcoli, P. Delugas, R. A. DiStasio Jr, A. Ferreti, A. Floris, G. Fratesi, G. Fugallo, R. Gebauer, U. Gerstmann, C. Gougoussis, F. Giustino, T. Gorni, J. Jia, M. Kawamura, H. Y Ko, A. Kokalj, E. Kkbenli, M. Lazzeri, M. Marsili, N. Marzari, F. Mauri, N. L. Nguyen, H. V. Nguyen, A. Otero-de-la-Roza, L. Paulatto, S. Ponc, D. Rocca, R. Sabatini, B. Santra, M. Schlipf, A. P. Seitsonen, A. Smogunov, I. Timrov, T. Thonhauser, P. Umari, N. Vast, X. Wu and S. Baroni. 2017 J. Phys.: Condens. Matter 29 465901.

[27] J. P. Perdew, K. Burke, and M. Ernzerhof, Phys. Rev. Lett. 77 (1996) 3865.

[28] H. J. Monkhorst and J. D. Pack, Phys. Rev. B 13 (1976) 5188.

[29] F. Birch, Phys. Rev. 71 (1947) 809.

[30] F. D. Murnaghan, Proc. Natl. Acad. Sci. USA. 30 (1944) 244.

[31] A. Dal Corso, J. of Phys.: Condens. Matter 28 (2016) 075401.

[32] Y. Le Page and P. Saxe, Phys. Rev. B. 65 (2002) 104104.

[33] I. Galanakis, P.H. Dederichs, N. Papanikolaou, Phys. Rev. B 66 (2002) 174429.

[34] A. Togo, Phonopy, http://phonopy.sourceforge.net/.

 doi:10.20944/preprints202211.0409.v1

[35] A. Togo, F. Oba, I. Tanaka, Phys. Rev. B 78 (2008) 134106.

[36] A. Togo, L. Chaput, I. Tanaka, G. Hug, Phys. Rev. B 81 (2010) 174301.

[37] L. Chaput, A. Togo, I. Tanaka, G. Hug, Phys. Rev. B 84 (2011) 094302.

[38] A. Togo, L. Chaput, I. Tanaka, Phys. Rev. B 91 (2015) 094306.

[39] A. Togo, I. Tanaka, Phys. Rev. B 87 (2013) 184104.

[40] N.J. Lane, S.C. Vogel, G. Hug, A. Togo, L. Chaput, L. Hultman, M.W. Barsoum, Phys. Rev. B 86 (2012) 214301.

[41] A. Togo, F. Oba, I. Tanaka, Phys. Rev. B 77 (2008) 184101.

[42] H. Akamatsu, K. Fujita, T. Kuge, A. Sen Gupta, A. Togo, S. Lei, F. Xue, G. Stone, J.M. Rondinelli, L.-Q. Chen, I. Tanaka, V. Gopalan, K. Tanaka, Phys. Rev. Lett. 112 (2014) 187602.

[43] J.M. Skelton, S.C. Parker, A. Togo, I. Tanaka, A. Walsh, Phys. Rev. B 89 (2014) 205203.

[44] A. Matsumoto, Y. Koyama, A. Togo, M. Choi, I. Tanaka, Phys. Rev. B 83 (2011) 214110.

[45] D.C. Wallace, Thermodynamics of Crystals, Dover Publications, 1998.